IEEE Sensors Council

# A Simulated Intelligent Pixelated Electrode Array for Surface Electromyography Sensors

Sakib Chowdhury, *Student Member, IEEE*, Dipayon Kumar Sikder, and Apratim Roy, *Member, IEEE*

***Abstract*—Surface electromyography (sEMG) is a noninvasive diagnostic tool for identifying muscle diseases, which is also utilized in portable smart devices to recognize body mass compositions. Human skin tissue composition varies from person to person. Therefore, the strength of muscle stimulation that reaches the skin surface varies with skin formation, resulting in a variation of signal-to-noise ratio (SNR). Electrodes used in sEMG have inherent filtering capabilities and the cutoff frequencies depend on the dimension of the electrodes. In this article, we propose a novel electrode array composed of tiny electrodes, mimicking the arrangement in high-density sEMG, that can modulate electrode size and leverage the natural filtering property of electrodes to maximize the SNR. The arrangement is similar to the arrangement of image pixels on a digital screen and hence called "pixelated." The proposed scheme is very adaptive to varied skin composition as well as body location and hence behaves like an intelligent agent. We used a statistical SNR prediction algorithm, which validated the proposed idea. While determining the ideal electrode layout, the suggested concept significantly reduces the signal sample duration and can avoid additional computational overhead once the optimal arrangement is identified. Moreover, it offers a substantial advantage over traditional signal processing techniques, which need constant processing to filter out noise and improve the intelligent signal with digital filters and transceiver amplifiers. Because of truncated processing cost, the proposed array is suitable for wearable devices driven with low-power embedded microcontrollers, where high computational requirement often proves to be prohibitive.**

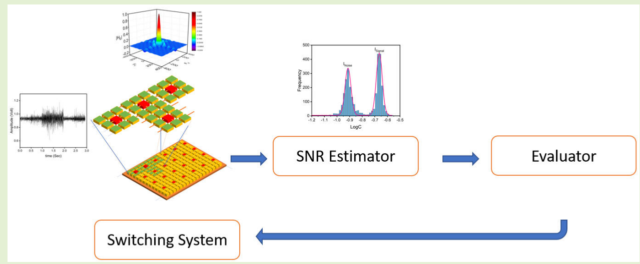


***Index Terms*— Biomedical application, electrodes, electromyography (EMG), signal processing.**

## I. INTRODUCTION

ELECTROMYOGRAPHY (EMG) is a fascinating field of biomedical science that delves into the intricacies of our body's electrical signals, providing valuable insights into muscle function and neuromuscular disorders. EMG acts as a key to understanding the connection between our nerves and muscles. It detects electrical signals during nerve stimulation, revealing how muscles generate tiny electrical currents before movement. Electrodes on the skin or comparable minimally invasive devices in the muscle can measure the EMG signal. Needle electromyography (nEMG) and surface electromyography (sEMG) are the two options for EMG measurements. Needle-shaped electrodes can directly measure electric potentials in the fibers, making nEMG more accurate than sEMG. sEMG is increasingly popular since it is noninvasive and may be given by nonmedical personnel without harming the patient [1].

The factors that have the greatest impact on the EMG signal fall into three primary categories [2], [3]. This classification is established so that EMG signal analysis methods may be optimized and consistent equipment can be created. First, the causative factors can be extrinsic or intrinsic. The extrinsic causative factors are the shape of the electrode, the distance between electrode detection surfaces, the location of the electrode relative to the motor points in the muscle, the location of the muscle electrode on the muscle surface relative to the lateral edge of the muscle, and the orientation of the detection surfaces relative to the muscle fibers. Physiological, anatomical, and biochemical factors are known to be intrinsic causative factors. The number of active motor units, fiber type composition, blood flow, fiber diameter, depth and location of active fibers, and amount of tissue between the surface of the muscle and the electrode are some intrinsic causative

Manuscript received 13 October 2023; revised 19 November 2023; accepted 18 December 2023. Date of publication 28 December 2023; date of current version 13 February 2024. The associate editor coordinating the review of this article and approving it for publication was Prof. Aime (GE) Lay-Ekuakille. *(Sakib Chowdhury and Dipayon Kumar Sikder contributed equally to this work.) (Corresponding author: Apratim Roy.)*

Sakib Chowdhury was with the Electrical and Electronic Engineering (EEE) Department, Bangladesh University of Engineering and Technology, Dhaka 1205, Bangladesh. He is now with the Stevens Institute of Technology, Hoboken, NJ 07030 USA (e-mail: sakibchowdhury131@gmail.com).

Dipayon Kumar Sikder was with the Electrical and Electronic Engineering (EEE) Department, Bangladesh University of Engineering and Technology, Dhaka 1205, Bangladesh. He is now with the Electrical and Systems Engineering (ESE) Department, Washington University in St. Louis, St. Louis, MO 63130 USA (e-mail: dipayonsikder@gmail.com).

Apratim Roy is with the Department of Electrical and Electronic Engineering, Bangladesh University of Engineering and Technology, Dhaka 1205, Bangladesh (e-mail: apratimroy@eee.buet.ac.bd).

Digital Object Identifier 10.1109/JSEN.2023.3345729

factors that influence EMG measurements. For example, a substantial layer of fat and skin tissue on top of muscle adds effective resistance between the fibers and the electrode. This impedance significantly attenuates the amplitude and changes the phases of the induced signal in the skin tissue compared to the original action potential [4], [5]. Physical and physiological phenomena that are influenced by one or more causal variables are intermediate factors. This may be due to the bandpass filtering characteristics of the electrode and its detection volume, the superposition of action potentials in the measured EMG signal, and the conduction velocity of the action potential that propagates across the muscle fiber membrane. Intermediate factors can be caused by even crosstalk from adjacent muscles. Deterministic factors are directly influenced by intermediate factors. The number of active motor units, motor firing rate, and mechanical interaction between muscle fibers are some deterministic factors that have a direct bearing on the information in the EMG signal [6].

sEMG is measured using a variety of methods, and the amplitude of the sEMG signal ranges from microvolts to low millivolts [6]. In addition, the sEMG signal's amplitude and temporal-frequency domain features are influenced by variables such as timing and intensity of muscle contraction, electrode's distance from the active muscle area, quality of overlaying adipose tissue, properties of electrode and amplifier, and quality of contact between electrode and skin [7]. The resulting variability of sEMG signal among patients can be decreased by putting the electrodes over the same skin region in subsequent recording sessions. Moreover, the issue of decreasing variability across participants can be addressed by techniques involving normalizing the EMG signal [8], [9]. Many of the pressing concerns regarding the collection and processing of sEMG signal have lately been addressed in a multinational consensus initiative known as SENIAM: sEMG for noninvasive assessment of muscles [10].

The ratio between the detected EMG signal and undesired noise contributions from the surroundings is frequently used to describe the quality of the measured EMG recording. Assuming that amplifier design and analog-to-digital (A/D) conversion method used in the sEMG instrument surpass acceptable requirements [11], this signal-to-noise ratio (SNR) is almost entirely dictated by the electrodes, where the parameters of the electrode–electrolyte–skin interface exert a dominating influence. Therefore, impedance consistency plays a crucial role in determining the accuracy of EMG measurements. While the role of the magnitude of muscle impedance on the SNR of the measured sEMG signal is not critical, the stability of impedance over time and the balance of impedance between electrode sites have a significant effect on this ratio, both in terms of noise levels and spatial resolution [10]. It is also critical that the electrode–skin impedance remains constant during the measuring period. The SNR, such as the spatial resolution of the recorded EMG signal, will wander if the impedance drifts during the time of measurement. Recent research suggests that the relative amount of electrode–skin impedance influences the energy of the recorded EMG signal. For example, compared to high electrode–skin impedance ($>100$ k$\Omega$), low interface impedance ($<10$ k$\Omega$) results in a higher level of energy for EMG frequency components below 100 Hz [7].

Due to the introduction of numerous artifacts or noise components, the identifying features of real EMG signal elements originating in the muscle are often lost. In addition, the characteristics of the EMG signal are determined by the subject's internal structure, which includes individual skin formation, blood flow velocity, skin temperatures, tissue structure (muscle/fat ratio), measurement site, and other factors. These influential factors are often responsible for generating various sorts of noise elements evident in EMG signals. This may also have an impact on the outcome of feature extraction and, as a result, the diagnosis made with EMG signals. Various noise removal approaches suitable for EMG signal capture have been developed, which address noise sources such as inherent noise in electrodes [12], movement artifacts [13], [14], electromagnetic noise [15], crosstalk [16], and electrocardiographic artifacts [17].

Mechanical disruption of the electrode charge layer and skin deformation cause surface electrode motion artifacts [18]. Electrodes relative to the skin cause motion artifacts. Recessed electrodes use conductive gel or paste to prevent this. The layer dampens mechanical disturbances from electrode–skin relative motion, minimizing signal interference. The second motion artifact is caused by skin potential. Reducing skin impedance eliminates this motion artifact, but recessed electrodes cannot [18]. Tam and Webster [14] suggested abrading the top skin layers to reduce skin impedance. Burbank and Webster [19] found that puncturing skin reduces skin impedance. Online and offline signal conditioning eliminates EMG motion artifacts [20]. The measuring equipment commonly includes a high-pass filter to remove the dominant frequency component in motion artifact power density, which is often less than 20 Hz. To avoid myoelectric signal loss, the filter's corner frequency is usually 10 Hz and should not exceed 20 Hz. Filtering may alter the original signal at frequencies approaching the cutoff frequency. Hamilton and Curley [21] investigated an adaptive skin impedance-based method for eliminating motion artifacts in ambulatory electrocardiography (ECG) recordings. The adaptive method reduced artifacts by 12.5 dB in preliminary tests, but skin stretch sensors were too expensive to employ. Ng et al. [22] introduced remote healthcare low-noise capacitive electromyography using the CEMG biosensor.

Signal recordings in EMG can be susceptible to interference from magnetic or electric power lines [18]. This susceptibility arises due to the closed loop formed by the electrode leads, the subject, and the signal amplifier. When a time-varying magnetic field passes through this loop, the electrode leads generate a current that is proportional to the time derivative of the field and the area enclosed by the loop. In addition, both the electrode leads and the subject become capacitively coupled to the surrounding electric field, resulting in the generation of small displacement currents in both. The interference potential at the electrodes is detected by the amplifier because the electrode impedance is lower than the amplifier's input impedance. This occurs as the subject's displacement current travels through the ground electrode via skin impedance, resulting in a common-mode voltage at the recording electrode. The differential amplifier should exclude any common-mode signal from the EMG signal when bipolar recording electrodes are used. In real-life recordings, the skin impedances at the two electrodes and the amplifier input impedances are not precisely matched, and the common-mode rejection ratio is finite [23]. The "driven right leg circuit" suggests active grounding to solve this problem [23], [24]. This circuit employs a feedback amplifier that sends the body's common-mode voltage negatively (phase reversed) to a third electrode, lowers it, and reduces power line interference. In a related study, Gokcesu et al. [25] and Robertson et al. [26] successfully utilized a real-time power line interference removal technique to boost SNR.

Even with suitable skin preparation at the electrode's recording locations and well-designed apparatus, power line interference in the acquired EMG signal may not be sufficiently attenuated, requiring offline processing to remove artifacts. A narrow fixed notch filter centered on the fundamental frequency can be used to filter the EMG (50 or 60 Hz). This method works well for simple biofeedback applications that require only an estimated amplitude estimation. Nevertheless, notch filtering will remove signal and power line components, affecting the spectrum content and signal waveform. Ferdjallah and Barr [27] introduced three adaptive digital notch filters to track and remove 60-Hz noise from biological data. Notwithstanding their advantages over fixed notch filters, adaptive filters still remove signal and noise from EMG signals. Baratta et al. [28] proposed a method for eliminating power line artifacts in time-domain EMG. It involves analyzing the fundamental frequency component of power line interference in a silent section of the recording and then subtracting a sinusoidal waveform with the same amplitude and phase as the interfering signal. This method assumes the constancy of the power line artifact's amplitude and phase during recording.

Our study addresses the tradeoff between electrode dimensions and noise reduction in an autonomous fashion. Increasing the dimension of electrodes will introduce a reduction in noise, while a decrease in the dimensions will preserve signal features up to many higher order frequencies. In this work, a novel pixelated electrode arrangement is proposed, which will be compatible with high-density sEMG sensors. The proposed method allows EMG sensors to modulate their effective surface area in order to maximize the SNR in multiple subjects having different types of tissue composition for skin and muscles. The investigated protocol can eliminate the effect of overlaying tissues and minimize the noise effect significantly. As the low-pass filtering effect caused by electrodes influences the features in both space and time of the observed sEMG signal, this method can eliminate noise elements of the measured EMG signal.

## II. Methodology

### A. Transfer Function

Fig. 1 shows a typical relationship between the unit action potential generated in the muscle and the potential produced on the skin. Here, all points in space may be characterized using cylindrical coordinates $(r, \phi, z)$ where $r$, $\phi$, and $z$ have their usual meaning in the cylindrical coordinate system. In this situation, $Z1$ is the axis of a muscle fiber. $(r, 0, 0)$ is the geometric center of the electrode in the cylindrical system. The potential generated on the surface of the muscle fiber (denoted as the cylindrical shape in Fig. 1) is $V(\mathrm{a}, z)$ where a is the radius of the muscle fiber. The electrical potential induced on top of the skin, assuming axial symmetry, is indicated by the symbol $V(r, z)$ where $r$ is the collective thickness of the skin and other fat tissue. The resulting impulse response and transfer function for circular electrodes are specified by (1) [29] and (2) [30]. For example, the following equation applies to the impulse response $h_E(x, y)$ of a circular electrode:

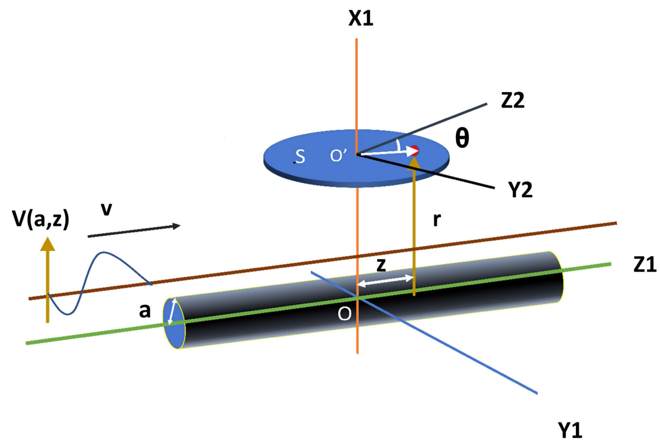


Fig. 1. Surface electrode model.

$$h_E = \begin{cases} \dfrac{1}{\pi r^2}, & \text{if } x^2 + y^2 \le r^2 \\ 0, & \text{otherwise} \end{cases} \tag{1}$$

where $r$ is the radius of the electrode.

The transfer function of a circular electrode in the frequency domain can be obtained from the Fourier transform of the previous equation

$$H_E(r, f_x, f_y) = \frac{2J_1\left(2\pi \cdot r \cdot \sqrt{f_x^2 + f_y^2}\right)}{2\pi \cdot r \cdot \sqrt{f_x^2 + f_y^2}} \tag{2}$$

where $f$ represents the frequency, $J_1(x)$ is the first-order Bessel function of the first kind, and $f_x$ and $f_y$ are the frequency component in the $x$- and $y$-directions [30]. On the other hand, the rectangular electrode has an impulse response $h_E(x, y)$, which takes the following form [31]:

$$h_E = \begin{cases} \dfrac{1}{ab}, & \text{if} - a/2 \le x \le a/2 \text{ and } -b/2 \le y \le b/2 \\ 0, & \text{otherwise} \end{cases} \tag{3}$$

where $a$ and $b$ are the sides of the electrode. The corresponding frequency-domain transfer function can also be found from its Fourier transform [31]

$$H_E(a, b, f_x, f_y) = \sin c(\pi a f_x) \cdot \sin c(\pi b f_y). \tag{4}$$

Fig. 2 shows the difference between the transfer functions of the two types of electrodes. It can be observed that

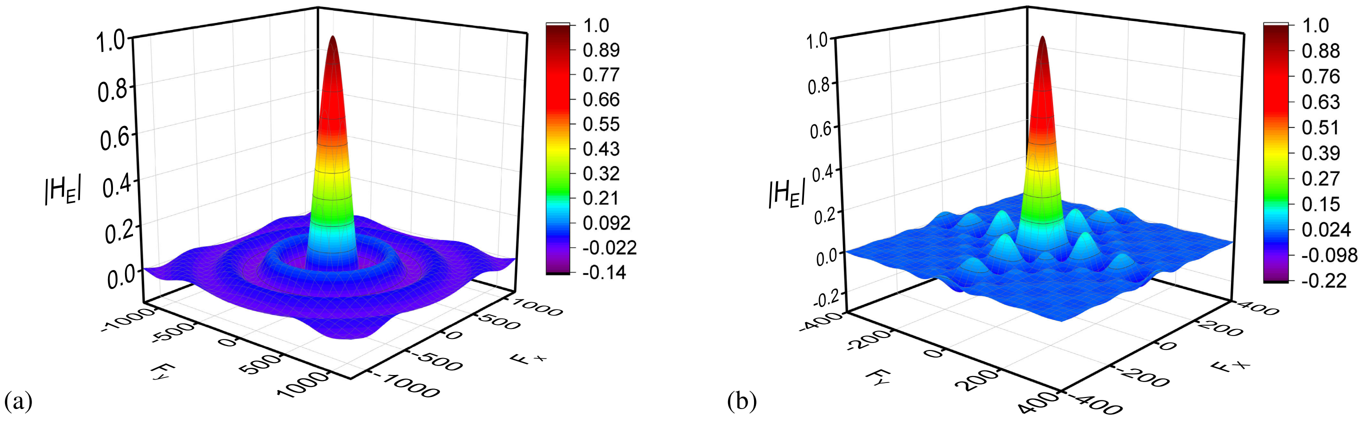


Fig. 2. Filtering effect for (a) circular electrode with 5 mm diameter and (b) rectangular electrode with 5-mm sides.

the circular electrode has larger unwanted ripples in the frequency distribution, whereas these unwanted components get largely suppressed by rectangular electrodes with similar spatial dimensions. For the proposed application, rectangular electrodes are chosen over circular electrodes since the former achieve better noise suppression with low interelectrode distance.

### B. Size Effect

Fig. 3 demonstrates how a change in size affects the performance achieved by the electrodes. As increasing the electrode dimension has a reciprocal relationship with the cutoff frequency allowed through the electrode, it allows manipulation of the electrode's inherent filtering capability. This property has been exploited in the presented work to modulate the cutoff point and eliminate irrelevant frequency components from the acquired signal.

This strategy may lead to smaller electrode areas being preferred as the low-pass filtering associated with electrode size has an impact on features in both space and time of the detected sEMG signal. However, a smaller electrode also lowers the SNR of the sEMG signal. Therefore, a compromise has to be achieved while choosing the area that can sufficiently satisfy the two conflicting requirements.

### C. Relationship Between Bandwidth and Electrode Length

The frequency-domain transfer function of the rectangular electrode in (4) can be manipulated to take the following form:

$$H_E(a, b, f_x, f_y) = \frac{\sin\{\pi(af_x + bf_y)\} + \sin\{\pi(af_x - bf_y)\}}{2\pi^2 ab f_x f_y}. \tag{5}$$

Now, at cutoff frequency, let us consider $f_x = f_{xc}$ and $f_y = f_{yc}$ and the impulse response should be equal to $(1/\sqrt{2})$. Furthermore, if we assume that a = b, the cutoff frequencies along both the axes become equal ($f_{xc} = f_{yc}$), and as a result, we arrive at (6) which represents an implicit function

$$\sin(2\pi a f_{xc}) = \sqrt{2}\pi^2 a^2 f_{xc}^2. \tag{6}$$

Consequently, by solving (6), the data of Fig. 4 are obtained that represents an inverse relationship between bandwidth and electrode length for a square electrode.

### D. Theory for Estimating SNR

To properly assess the best electrode configuration, an assessment tool is required that can distinguish between different qualities of signal condition. In this work, SNR has been adopted as a judgment factor to evaluate electrode arrangements. The SNR estimation method is based on article by Agostini and Knaflitz [32]. In this method, a time series $\{X_i\}$ is considered where $i = 1, 2, \ldots, N$ with $N$ the number of samples. The time series has a sampling frequency of 2000 Hz and a duration of 30 s. Thus, the number of samples ($N$) is 60 000 (2000 × 30). Thereafter, the series $\{X_i\}$ is divided into $M$ $(= N/r)$ epochs where $r$ has value of 10. Thus, the series takes the form of

$$\{X_{kj}\} = \{X_{1j}, X_{2j}, \ldots, X_{Mj}\}, \quad j = 1, 2, \ldots, 10.$$

We now obtain the auxiliary time series representing the normalized sum of squares by the following equation:

$$C(k) = \sum_{j=1}^{10} \frac{X_{kj}^2}{10}, \quad k = 1, \ldots, M. \tag{7}$$

After obtaining the histogram of the series as $\log_{10} C$, the bins of the histogram are defined as

$$\mathrm{bins}(m) = m \cdot \frac{\max(\log_{10} C) - \min(\log_{10} C)}{2.N\mathrm{bins}} + \min(\log_{10} C)$$
$$\text{Here, } m = 1, 3, \ldots, 2, N\mathrm{bins} - 1 \tag{8}$$

where $N$bins represents the number of bins.
In general, selecting between 50 and 100 bins is a reasonable decision [32].

We now look for local maxima in the curve that interpolates the histogram's frequencies, as shown in Fig. 5. The absolute maximum and the highest relative maximum are then determined. In Fig. 5(b), the maximum point on the left is related to noise ($I_{\mathrm{noise}}$), whereas the maximum point on the right is associated with signal ($I_{\mathrm{signal}}$). Here, $I$ represents an intermediate parameter that has no physical significance.

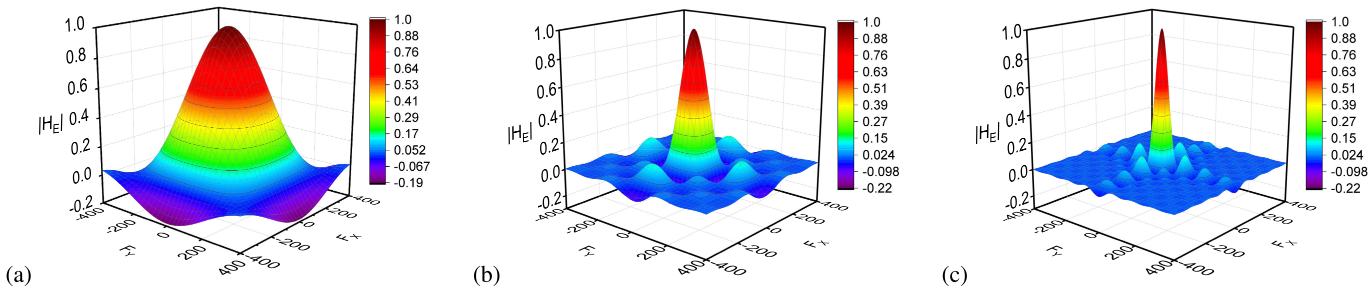


Fig. 3. Low-pass filtering effect achieved by rectangular electrode depending on sides $a$ and $b$. (a) $a = b = 1$ mm. (b) $a = b = 3$ mm. (c) $a = b = 6$ mm.

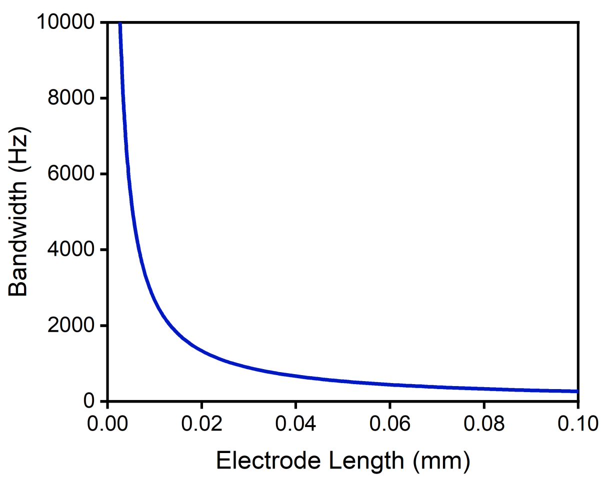


Fig. 4. Relationship between bandwidth and electrode length for a square electrode.

Averaging five bins around $I_{\text{noise}}$, the mean power of noise is estimated as

$$P_{\text{noise}} = \frac{\sum_{i=I_{\text{noise}}-2}^{I_{\text{noise}}+2} \text{bins}(i).\text{freq}(i)}{\sum_{i=I_{\text{noise}}-2}^{I_{\text{noise}}+2} \text{freq}(i)} \tag{9}$$

and the root-mean-square value of background noise $e_{\text{noise}}$ can be defined as

$$e_{\text{noise}} = \sqrt{P_{\text{noise}}}. \tag{10}$$

Finally, the SNR is estimated in decibels with the help of

$$\text{SNR} = 10.\log_{10} \frac{P_{\text{signal}} - P_{\text{noise}}}{P_{\text{noise}}}. \tag{11}$$

## E. Intelligent Pixelated Electrode Array

A novel pixelated electrode arrangement is proposed in this work that can change the effective size of the electrode by arranging them in an array and connecting them through ultrahigh conductive electronic switches. The purpose of this article is to demonstrate the working principle of the proposed electrode arrangement in a simulation environment. The practical implementation of this electrode is out of the scope of this article. Since this experiment is done in a simulated environment, we used a publicly available EMG dataset, which is electromyographic stimulations recorded from multiple volunteers. We demonstrate that the output signal of the proposed system has a higher SNR compared to the SNR of the original signal. Since each electrode element itself can function as an inherent low-pass filter, this property is utilized to regulate noise levels from the EMG records. From Fig. 4, it was evident that changing the electrode size can effectively modulate the cutoff point and the allowed bandwidth through the electrode. By leveraging this feature, the base setting of the intelligent electrode array is established. The proposed electrode arrangement is termed pixelated as it employs unit pixel-type elements with size in micrometer level instead of using one large electrode. Fig. 6 shows the proposed electrode array arrangement with details where each pixelated electrode is connected to its neighboring pixels through ultralow resistivity electronic switches. As the size dependence of the cutoff frequency shown Fig. 3, it was clearly observed that as the electrode becomes larger, it gets more and more frequency selective. Therefore, instead of collecting all frequency components, the required area of bandwidth can be focused on through adjusting the effective electrode size. Moreover, this strategy is expected to eliminate most of the noise components from the signal and hence increase the SNR. However, with significantly large dimensions, the electrode will no longer capture ac components of the emerged EMG signal and rather receive only dc elements. Thus, with an increase in effective electrode surface area, the SNR will reach a maximum attainable level and start to decrease afterward. This setting at the maximum SNR level is considered as the optimum setting of electrode sizes under the specified set of application conditions.

At the beginning of the operation, the setup has to go through a calibration phase that will perform the operations described above and find the optimum electrode setting. This calibration phase takes place in five sequential steps, which are discussed as follows.

1) *Step 1:* All the interlinked electronic switches are turned off so that each electrode pixel can function individually. In this setting, the effective electrode length is $\phi$, as shown in Fig. 6. An ADC will sample signal content from the $\phi$ sized electrodes and estimate SNR through the algorithm shown in Section II-D.
2) *Step 2:* Since the electrode response is highly dependent on shape, square electrodes are considered over circular electrodes to ensure minimum interelectrode distance. At the $n$th iteration, the CPU will electronically connect

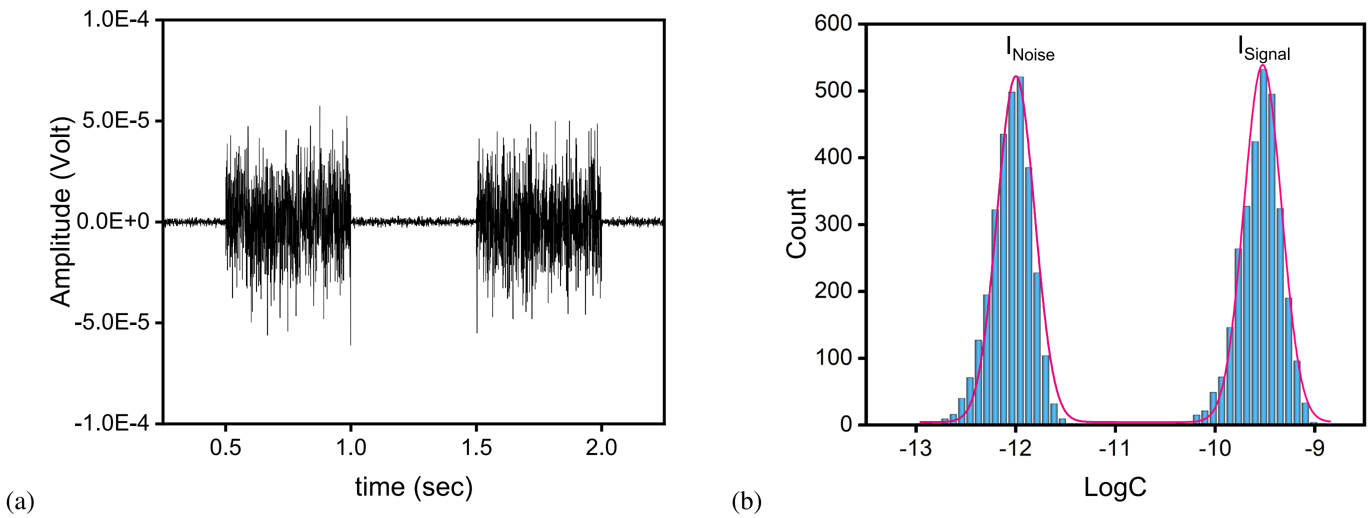


Fig. 5. (a) Amplitude versus time series graph of a synthetic EMG signal truncated to $t = 3$ s with SNR = 25 dB. (b) Histogram of $\mathrm{Log}_{10} C$ with $e_{noise} = 1\mu V$, SNR = 25 dB. The blue bars represent the bins that the algorithm uses to estimate the parameters.

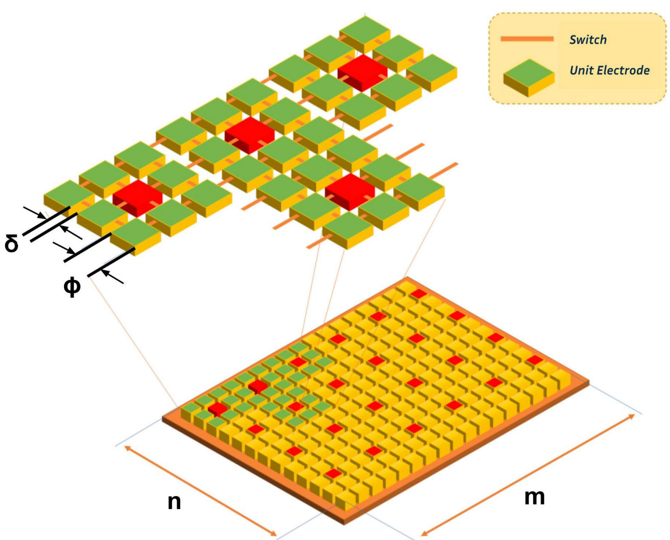


Fig. 6. Pixelated electrode array: the orange colored strips are ultrahigh conductive electronic gates. The red-colored electrodes are the center electrodes and the green-colored ones are the peripheral electrodes. Here, $\delta$ signifies the interelectrode distance, while $\phi$ signifies the size of each pixel.

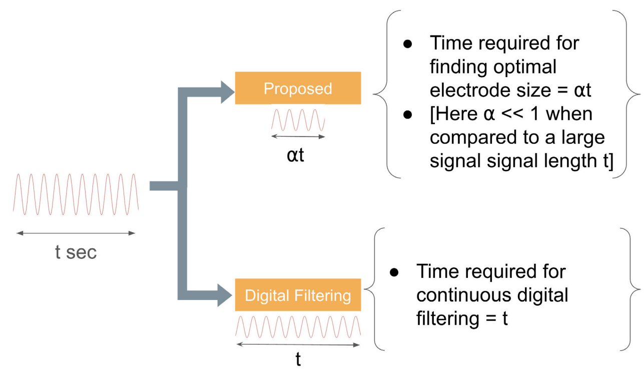


Fig. 7. Benefit of our proposed mechanism compared to digital filtering techniques.

$n^2$ electrodes to maintain a square shape. At this stage, the effective electrode length is $n * \phi$.

3) *Step 3:* At this stage, the SNR level of $n * \phi$ sized electrodes is calculated through the method discussed in Section II-D.
4) *Step 4:* Afterward, the CPU will evaluate whether the current SNR level is better than the $(n-r-1)$th iteration where $r$ is the memory parameter of the system. Thus, the CPU has to store the SNR levels of previous $r$ number of iterations in the memory. If the current SNR level is better than the previous iterations, the CPU will again go to Step 2. Otherwise, it will move to Step 5.
5) *Step 5:* The best achievable SNR is obtained as $\max(\mathrm{SNR}_{n-r-1}, \mathrm{SNR}_{n-r}, \mathrm{SNR}_{n-r+1}, \ldots, \mathrm{SNR}_{n-1})$ and the electrode size with best SNR level is considered as the optimum setting under the specified application conditions.

### F. Benefits of the Proposed Method

The proposed mechanism uses only a fraction of the infinite time series signal to calculate and determine the optimal electrode setup. In Fig. 7, $\alpha$ denotes the fraction of time series data $t$ that is required for finding optimal electrode configuration. For a significantly large signal (for continuous health monitoring), $\alpha \ll 1$. Thus, computation power is needed only for $\alpha t$ seconds, whereas, in the traditional digital filtering method, continuous processing is required. This makes our proposed method a good candidate for low-power health monitoring systems.

## III. Experimental Setup

Our experiment was done in the simulation environment. The software was built on python. The properties of the electrodes are mimicked with the transfer functions derived in Section II. To measure the performance of the SNR estimator, synthetic EMG signals were generated with additive white Gaussian noise by varying amplitude to mimic muscle contraction and muscle stimulation.

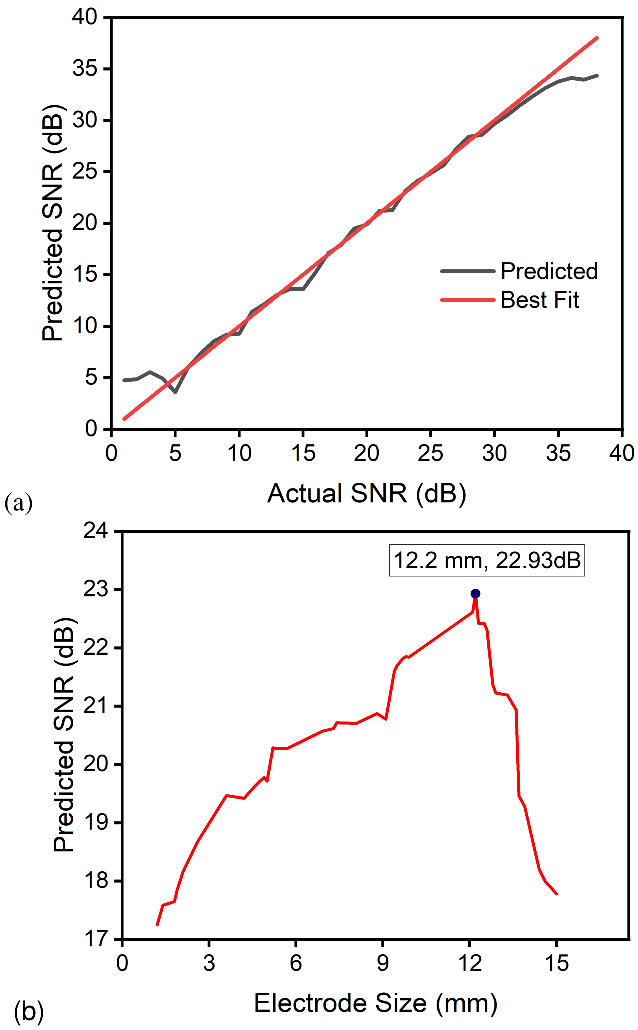


Fig. 8. (a) Performance analysis of the SNR estimator: the SNR level can be estimated with high accuracy within the wide range of 4–32 dB. (b) Finding the optimal electrode size for achieving maximum SNR level.

To validate the proposed algorithm, we tested the method on the putEMG dataset [33]. We considered signals from the database to be action potentials generated in the muscle fiber. Our algorithm estimated the best achievable SNR for signals from various patients. The optimal dimension of the electrode is also calculated by the scheme.

## IV. Results and Observation

This section is divided into two segments. The first segment discusses the accuracy and effective region of the SNR estimator, which is used to validate the proposed scheme. The second segment focuses on the performance of the proposed scheme based on the SNR values obtained from the SNR estimator. We find that, within the optimal operation range of the SNR estimator, our proposed scheme increases the SNR of the EMG signal. However, the SNR does not increase indefinitely, it drops after a certain peak value, and this peak value is considered as the maximum SNR that our proposed scheme can provide. However, we cannot provide any comparison with other SNR improving electrodes available in the market since our proposed scheme is entirely a new idea and similar ideas have never been implemented before.

### A. Performance of SNR Estimator

To analyze the performance of the SNR estimator, a synthetic signal with varying SNR level is generated, which is shown in Fig. 5. The higher amplitude segments of the synthetic signal signify muscle unit action potential during muscle contraction or expansion. In contrast, the lower amplitude segments in the EMG signal represent the condition of muscle relaxation. Here, synthetic cyclic signal segments with a length of 30 s are created, which have a cycle time of 1 s. They are produced by combining a random process that mimics noise level with a sequence that models the SMES generated during muscle activity. Background noise is generated as a Gaussian process with zero mean and a standard deviation of 1 V, whereas the SMES flash is created as a Gaussian sequence with zero mean and a standard deviation of $10^{(\mathrm{SNR}/20)} * 1$ V.

The SNR level of the synthetic signals is varied, while the predicted SNR level is compared with the actual reading. The resulting performance is demonstrated in Fig. 8(a) where the red line represents the theoretically best possible performance and the blue curve visualizes the estimator's readings. From Fig. 8(a), it is evident that the estimator remains highly accurate within a wide SNR range (from 4 to 32 dB). The performance of the SNR estimator for real-life data is very satisfactory and maintains consistency.

### B. Optimum Electrode Setting

As the source of real-life EMG signal datasets, the putEMG database has been used in this work. The putEMG dataset provides signals for 44 patients. Fig. 9(a) shows a sample EMG signal included in the dataset. The sampled signal is passed through the pixelated electrode array and the output from the arrangement is passed on to the SNR estimator. Fig. 9(b) shows the histogram plot of $\log C$ values calculated during SNR estimation as discussed in Section III. It is evident that the histogram plot produces features that match the plot generated with the synthetic signals. Here, two peaks remain visible in the plot where the left peak corresponds to $I_{\mathrm{noise}}$ and the right one corresponds to $I_{\mathrm{signal}}$. Ultimately, the SNR estimator estimates the SNR level with the help of the histogram plot.

The algorithm to obtain the optimal electrode setting is employed several times on the same signal while varying the electrode size by $\phi$ units as was shown in Fig. 6. For each size setting, the SNR estimator provides a predicted SNR value, which is considered acceptable if it lies within the high accuracy range presented in Fig. 8(a). The estimated SNR readings with varying electrode settings are shown in Fig. 8(b) where it can be observed that the SNR level reaches a maximum value of 23 dB at an electrode setting of 12.1 mm. Afterward, the SNR level decreases with size because, and with increased length, the electrode becomes highly frequency selective and eliminates intelligent signal elements while keeping unwanted signals such as dc components. Once the

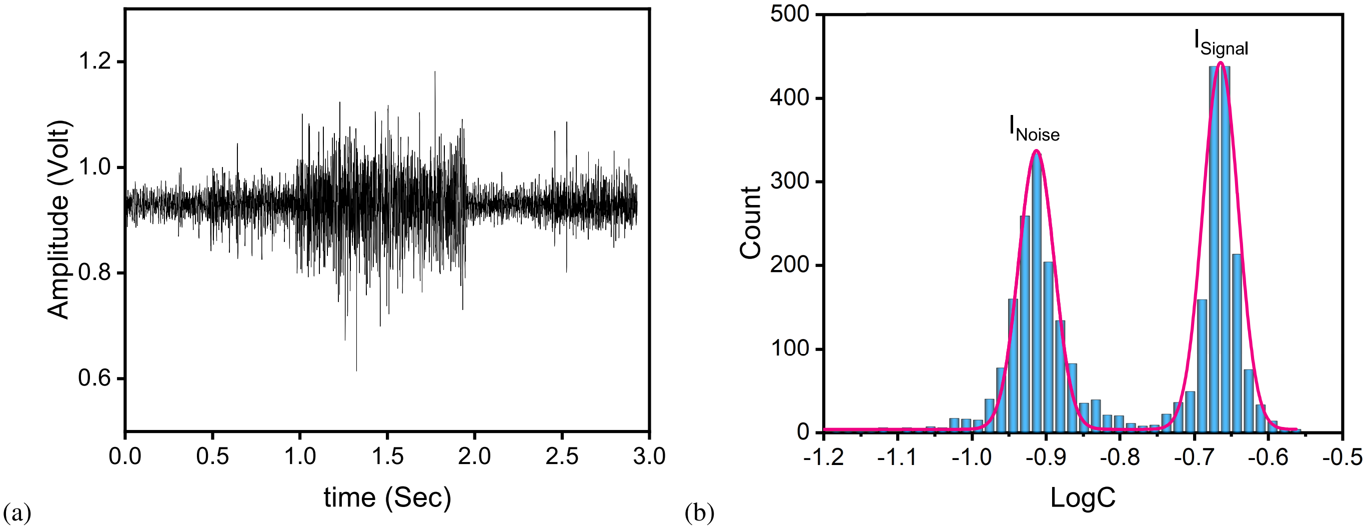


Fig. 9. (a) Sample signal from putEMG dataset: higher amplitude denotes muscle stimulation, while lower amplitude depicts muscle relaxation. (b) HHistogram plot of *LogC* values obtained from the putEMG dataset sample.

TABLE I
OPTIMAL ELECTRODE SETTING OF SAMPLES OF PUTEMG [33] DATASET

| Best achievable SNR (dB) | Electrode Length (mm) | Total Connected Pixels in X axis |
|---|---|---|
| 22.8 | 12.1 | 121 |
| 23.2 | 11.6 | 116 |
| 21.1 | 12.3 | 123 |
| 20.3 | 10.9 | 109 |
| 22.6 | 9.7 | 97 |
| 20.7 | 9.6 | 96 |
| 21.2 | 11.5 | 115 |

optimal electrode setting is found, the states of the electronic switches can be stored and no further computational overhead will be spent to maximize SNR level.

In Table I, the results obtained from seven different patients on putEMG [33] dataset are shown. We considered the time series signals from the putEMG dataset as action potentials generated on the muscle fiber. By estimating the SNR level through the SNR predictor and following the proposed scheme, the best achievable SNR level [as can be visualized from Fig. 8(b)] is determined. Our scheme provides the optimal electrode dimension to achieve this maximum SNR level. In our experimentation, each pixel electrode was considered to be 100 $\mu$m. Dividing the optimal electrode dimension by the size of each pixel electrode, one can calculate the total number of pixel electrodes to be connected.

In the proposed algorithm, the circular and rectangular surface electrode model and SNR estimator have been employed to carry out an independent analysis of sEMG signal for intelligent and low-overhead SNR optimization. As examples of ultralow resistive switches mandated in the design, GaN heterojunction field-effect transistor (HFET) switch having a gate length of 1 $\mu$m and gate width of 40 mm could provide a resistance of 20 m$\Omega$ [34]. A gate totem pole of bare 50-m$\Omega$ 30-V Si NMOSFETs (STN4NF03L) could be incorporated into GaN HFET half-bridge multichip modules (MCMs) in order to considerably minimize both gate resistance and inductance [34]. In addition, a new 900-V, 10-m$\Omega$ SiC MOSFET chip has been demonstrated, tested, and assembled with only 1.25–2.5-m$\Omega$ ON-resistance at 25 °C in a >400 A, half-bridge power module, depending on the number of chips per switch position (i.e., eight or four). The SiC MOSFET chip has reported a measured breakdown voltage >1 kV and a specific $R_{\mathrm{DS}}(\mathrm{ON})$ of 2.3 m$\Omega\cdot$cm$^2$. It was possible to assemble the chips in 16 power modules and characterize them up to 175 °C [35].

## V. FUTURE WORK

This article demonstrates a simulated intelligent electrode array capable of improving the SNR level of the acquired EMG signal. The practical implementation for this pixelated electrode design is beyond the scope of this article. However, further work is required to make substantial improvements in the proposed scheme. Even though the proposed scheme has been validated with real-life data, future research could involve evaluating the performance and potential limitations of the electrode array in real-world scenarios with the EMG data from a diverse group of individuals. An advanced machine learning algorithm can be used in the future in order to estimate SNR, detect and categorize muscle activity, and uncover patterns in the data. The proposed scheme has the potential to be integrated with prosthetic devices, which can provide more natural and accurate movement [36]. In the proposed scheme, the pixel electrodes are connected with ultralow resistive switches that can be made using nanomaterials such as graphene, carbon nanotubes, or metal oxide nanoparticles [37]. Moreover, MEMS technology might be utilized to incorporate ultralow resistance switches into the electrode array. MEMS switches can be fabricated using standard semiconductor processing techniques and can be integrated directly into the electrode array [38]. While the focus of the current study is on sEMG sensors, the pixelated electrode array could also be utilized for other applications, such as electroencephalography (EEG) and ECG [39].

TABLE II
COMPARISON BETWEEN SNR (dB) AFTER ACQUIRING DATA WITH SQUARE ELECTRODE AND PIXELATED ELECTRODE ARRAY [33]

| Actual Signal SNR (dB) | SNR(dB) after proposed scheme |
|---|---|
| 13.36 | 22.93 |
| 14,92 | 19.66 |
| 16.86 | 20.47 |
| 15.23 | 23.24 |
| 14.44 | 21.86 |
| 16.78 | 20.21 |

## VI. COMPARISON

Table II shows substantial improvement over the traditional square electrode while using our pixelated electrode array system. The field on the first column specifies the SNR level of the EMG signal taken by a square electrode from the subject's forearm. The benchmarking process utilized the idle hand gesture data of six healthy, nondisabled patients extracted from the putEMG dataset [33]. For different patients, the improvement of SNR by our proposed scheme ranges from 20.4% to 71.41%. The differences in percent improvement are unique due to the unique arrangement of pixelated electrodes for each patient's EMG signal. For each patient, the optimum electrode setting for maximizing SNR level is different. The second column from Table II shows the maximum achievable SNR from our scheme. This phenomenon can be largely attributed to the natural filtering property of square electrodes. In contrast to a related study by Velasco-Bosom et al. [40], which utilized a 4 × 4 array of 1.5 × 1.5 mm electrodes fabricated with PEDOT:PSS composites material for high-quality spatiotemporal EMG recordings, our focus is on optimizing SNR rather than achieving mm spatial resolution. Velasco-Bosom et al. [40] reported a peak SNR of 15.6 dB during the movement of the middle finger, but direct comparison is challenging due to differences in the locations of EMG measurements and variations in the experimental setup. Another study by Kim et al. [41] introduced a stretchable sEMG sensor array with SNR values of 9.18 (water attachment) and 20.77 dB (conductive gel attachment). However, the experimental environment and dataset differ significantly from ours, making direct conclusions inappropriate.

Our approach stands out in its emphasis on SNR optimization, showcasing patient-specific improvements and distinct advantages over existing studies. While spatial resolution is crucial in some applications, our tailored focus on SNR enhancement provides valuable contributions to the field of EMG signal processing.

## VII. CONCLUSION

This article presents an algorithm for optimizing the SNR of sEMG signals. It was evaluated with a putEMG dataset intended for assessing hand gesture recognition methods using the sEMG signal. As demonstrated by the obtained results, the proposed intelligent pixelated electrode arrangement enables precise and stable measurement of effective electrode length and, consequently, the number of electrodes required to be switched on for real-world applications. In addition, the proposed SNR estimator performs exceptionally for SNR values between 4 and 32 dB (Fig. 8). Although there is room for improvement in the design for a more precise estimator, the optimum and satisfactory performance indicate that the presented approach would be effective in future applications involving operator-independent processing of comparable biomedical signals.

## REFERENCES


[1] A. Merlo and I. Campanini, "Technical aspects of surface electromyography for clinicians," *Open Rehabil. J.*, vol. 3, no. 1, pp. 98–109, Jan. 2010.

[2] M. B. I. Reaz, M. S. Hussain, and F. Mohd-Yasin, "Techniques of EMG signal analysis: Detection, processing, classification and applications," *Biol. Procedures Online*, vol. 8, no. 1, pp. 11–35, Dec. 2006.

[3] P. Konrad, "The ABC of EMG—A practical introduction to kinesiological electromyography," Version 1.4, Mar. 2005, vol. 1, pp. 5–30.

[4] T. A. Kuiken, M. M. Lowery, and N. S. Stoykov, "The effect of subcutaneous fat on myoelectric signal amplitude and cross-talk," *Prosthetics Orthotics Int.*, vol. 27, no. 1, pp. 48–54, 2003.

[5] P. Bartuzi, T. Tokarski, and D. Roman-Liu, "The effect of the fatty tissue on EMG signal in young women," *Acta Bioeng. Biomechanics*, vol. 12, no. 2, pp. 87–92, 2010.

[6] C. J. De Luca, "The use of surface electromyography in biomechanics," *J. Appl. Biomech.*, vol. 13, no. 2, pp. 135–163, May 1997.

[7] S. Day, "Important factors in surface EMG measurement," Bortec Biomedical Ltd., Calgary, AB, Canada, Tech. Rep., 2002, pp. 1–17.

[8] Y. Zhao et al., "Flexible and wearable EMG and PSD sensors enabled locomotion mode recognition for IoHT-based in-home rehabilitation," *IEEE Sensors J.*, vol. 21, no. 23, pp. 26311–26319, Dec. 2021.

[9] A. S. Asheghabadi, S. B. Moqadam, and J. Xu, "Multichannel finger pattern recognition using single-site mechanomyography," *IEEE Sensors J.*, vol. 21, no. 6, pp. 8184–8193, Mar. 2021.

[10] H. J. Hermens et al., "European recommendations for surface electromyography," *Roessingh Res. Dev.*, vol. 8, no. 2, pp. 13–54, 1999.

[11] B. Gerdle, S. Karlsson, S. Day, and M. Djupsjöbacka, "Acquisition, processing and analysis of the surface electromyogram," in *Modern Techniques in Neuroscience Research*. Cham, Switzerland: Springer, 1999, pp. 705–755.

[12] X. Navarro, T. B. Krueger, N. Lago, S. Micera, T. Stieglitz, and P. Dario, "A critical review of interfaces with the peripheral nervous system for the control of neuroprostheses and hybrid bionic systems," *J. Peripheral Nervous Syst.*, vol. 10, no. 3, pp. 229–258, Sep. 2005.

[13] E. A. Clancy, E. L. Morin, and R. Merletti, "Sampling, noise-reduction and amplitude estimation issues in surface electromyography," *J. Electromyogr. Kinesiol.*, vol. 12, no. 1, pp. 1–16, Feb. 2002.

[14] H. Tam and J. G. Webster, "Minimizing electrode motion artifact by skin abrasion," *IEEE Trans. Biomed. Eng.*, vol. BME-24, no. 2, pp. 134–139, Mar. 1977.

[15] M. Malboubi, F. Razzazi, and S. M. Aliyari, "Elimination of power line noise from EMG signals using an efficient adaptive Laguerre filter," in *Proc. ICSES Int. Conf. Signals Electron. Circuits*, Sep. 2010, pp. 49–52.

[16] Y. Blanc and U. Dimanico, "Electrode placement in surface electromyography (sEMG) 'minimal crosstalk area' (MCA)," *Open Rehabil. J.*, vol. 3, no. 1, pp. 110–126, 2010.

[17] G. Lu et al., "Removing ECG noise from surface EMG signals using adaptive filtering," *Neurosci. Lett.*, vol. 462, no. 1, pp. 14–19, Sep. 2009.

[18] J. G. Webster, "Reducing motion artifacts and interference in biopotential recording," *IEEE Trans. Biomed. Eng.*, vol. BME-31, no. 12, pp. 823–826, Dec. 1984.

[19] D. P. Burbank and J. G. Webster, "Reducing skin potential motion artefact by skin abrasion," *Med. Biol. Eng. Comput.*, vol. 16, no. 1, pp. 31–38, Jan. 1978.

[20] R. Chowdhury, M. Reaz, M. Ali, A. Bakar, K. Chellappan, and T. Chang, "Surface electromyography signal processing and classification techniques," *Sensors*, vol. 13, no. 9, pp. 12431–12466, Sep. 2013.

[21] P. S. Hamilton and M. G. Curley, "Adaptive removal of motion artifact," in *Proc. 19th Annu. Int. Conf. IEEE Eng. Med. Biol. Society. Magnificent Milestones Emerg. Opportunities Med. Eng.*, Oct. 1997, pp. 297–299.

[22] C. L. Ng, M. B. I. Reaz, and M. E. H. Chowdhury, "A low noise capacitive electromyography monitoring system for remote healthcare applications," *IEEE Sensors J.*, vol. 20, no. 6, pp. 3333–3342, Mar. 2020.

[23] B. B. Winter and J. G. Webster, "Reduction of interference due to common mode voltage in biopotential amplifiers," *IEEE Trans. Biomed. Eng.*, vol. BME-30, no. 1, pp. 58–62, Jan. 1983.

[24] M. R. Neuman and J. Webster, "Biopotential amplifiers," in *Medical Instrumentation: Application and Design*, vol. 4. Hoboken, NJ, USA: Wiley, 1998, pp. 241–292.

[25] K. Gokcesu, M. Ergeneci, E. Ertan, and H. Gokcesu, "An adaptive algorithm for online interference cancellation in EMG sensors," *IEEE Sensors J.*, vol. 19, no. 1, pp. 214–223, Jan. 2019.

[26] D. G. E. Robertson, G. E. Caldwell, J. Hamill, G. Kamen, and S. Whittlesey, *Research Methods in Biomechanics*. Champaign, IL, USA: Human Kinetics, 2013.

[27] M. Ferdjallah and R. E. Barr, "Adaptive digital notch filter design on the unit circle for the removal of powerline noise from biomedical signals," *IEEE Trans. Biomed. Eng.*, vol. 41, no. 6, pp. 529–536, Jun. 1994.

[28] R. V. Baratta, M. Solomonow, B.-H. Zhou, and M. Zhu, "Methods to reduce the variability of EMG power spectrum estimates," *J. Electromyogr. Kinesiol.*, vol. 8, no. 5, pp. 279–285, Oct. 1998.

[29] J.-N. Helal and P. Bouissou, "The spatial integration effect of surface electrode detecting myoelectric signal," *IEEE Trans. Biomed. Eng.*, vol. 39, no. 11, pp. 1161–1167, Nov. 1992.

[30] E. Stein and G. Weiss, *Introduction to Fourier Analysis on Euclidean Spaces*. Princeton, NJ, USA: Princeton Univ. Press, 1971.

[31] B. Afsharipour, S. Soedirdjo, and R. Merletti, "Two-dimensional surface EMG: The effects of electrode size, interelectrode distance and image truncation," *Biomed. Signal Process. Control*, vol. 49, pp. 298–307, Mar. 2019.

[32] V. Agostini and M. Knaflitz, "An algorithm for the estimation of the signal-to-noise ratio in surface myoelectric signals generated during cyclic movements," *IEEE Trans. Biomed. Eng.*, vol. 59, no. 1, pp. 219–225, Jan. 2012.

[33] P. Kaczmarek, T. Mańkowski, and J. Tomczyński, "PutEMG—A surface electromyography hand gesture recognition dataset," *Sensors*, vol. 19, no. 16, p. 3548, Aug. 2019. [Online]. Available: https://www.mdpi.com/1424-8220/19/16/3548

[34] B. Hughes et al., "Normally-off GaN switching 400V in 1.4 ns using an ultra-low resistance and inductance gate drive," in *Proc. 1st IEEE Workshop Wide Bandgap Power Devices Appl.*, Oct. 2013, pp. 76–79.

[35] J. Casady et al., "Ultra-low (1.25 m) on-resistance 900V SiC 62 mm Half-bridge power modules using new 10 m SiC MOSFETs," in *Proc. PCIM Eur. Int. Exhib. Conf. Power Electron., Intell. Motion, Renew. Energy Energy Manage.*, May 2016, pp. 1–8.

[36] M. P. Selvan, R. Raj, R. Gowtham Sai, S. Jancy, and V. A. Mary, "Prosthetic hand using EMG," *J. Phys., Conf. Ser.*, vol. 1770, no. 1, Mar. 2021, Art. no. 012018.

[37] Y. Wu, Y. Chai, H.-Y. Chen, S. Yu, and H.-S. P. Wong, "Resistive switching AlOx-based memory with CNT electrode for ultra-low switching current and high density memory application," in *Proc. Symp. VLSI Technol.*, Jun. 2011, pp. 26–27.

[38] Kurmendra and R. Kumar, "Materials selection approaches and fabrication methods in RF MEMS switches," *J. Electron. Mater.*, vol. 50, no. 6, pp. 3149–3168, Jun. 2021.

[39] N. Pakniyat, M. Soundirarajan, S. Gohari, C. Burvill, O. Krejcar, and H. Namazi, "Decoding of facial muscle-brain relation by information-based analysis of electromyogram (EMG) and electroencephalogram (EEG) signals," *Waves Random Complex Media*, pp. 1–10, Oct. 2021.

[40] S. Velasco-Bosom et al., "Conducting polymer-ionic liquid electrode arrays for high-density surface electromyography," *Adv. Healthcare Mater.*, vol. 10, no. 17, Sep. 2021, Art. no. 2100374.

[41] N. Kim, T. Lim, K. Song, S. Yang, and J. Lee, "Stretchable multichannel electromyography sensor array covering large area for controlling home electronics with distinguishable signals from multiple muscles," *ACS Appl. Mater. Interfaces*, vol. 8, no. 32, pp. 21070–21076, Aug. 2016.


**Sakib Chowdhury** (Student Member, IEEE) received the bachelor's degree in electrical and electronic engineering from the Bangladesh University of Engineering and Technology, Dhaka, Bangladesh, in 2022.

He was a part-time Research Assistant with the Bangladesh University of Engineering and Technology. He is a Provost's Doctoral Fellow at the Electrical and Computer Engineering Department, Stevens Institute of Technology, Hoboken, NJ, USA. He is also working as an AI Research Engineer at Celloscope-bd, Dhaka. His research interests include biomedical signal processing, computer vision, and natural language processing.

**Dipayon Kumar Sikder** received the bachelor's degree in electrical and electronic engineering from the Bangladesh University of Engineering and Technology, Dhaka, Bangladesh, in 2022. He is pursuing the Ph.D. degree with the Department of Electrical and Systems Engineering, Washington University in St. Louis, St. Louis, MO, USA.

He was a Faculty Member at Leading University, Sylhet, Bangladesh. He is a Graduate Research Fellow with Washington University in St. Louis. His research interests include nanoresonators, light-trapping nanostructures, optoelectronic devices, and biomedical applications.

**Apratim Roy** (Member, IEEE) is a Professor of Electrical and Electronic Engineering at the Bangladesh University of Engineering and Technology (BUET), Dhaka, Bangladesh. He has coauthored over 30 research papers in peer-reviewed journals and international conferences. His research interests include biomedical systems, nanoelectronics, and radio frequency integrated circuit (RFIC) design.

Dr. Roy received several best paper awards, including one at International Conference on Telecommunications and Signal Processing (TSP), in 2021. He has served on the Program Committee for International Conference on Electronics and Communication Engineering (ICECE) in 2022, 2020, and 2018; and the IEEE R10 HTC in 2017. He is a U.S. State Department Alumni.